Available online at www.sciencedirect.com
ScienceDirect
Solid State Ionics 178 (2007) 1608–1616
SOLID STATE IONICS
www.elsevier.com/locate/ssi

Preparation and characterization of IrO_2–YSZ nanocomposite electrodes by MOCVD

A.M. Torres-Huerta [a,b,*], J.R. Vargas-García [a], M.A. Domínguez-Crespo [c]

[a] *Instituto Politécnico Nacional, Departamento de Metalurgia y Materiales, A.P. 75-874, 07300 México, D.F. Mexico*
[b] *Universidad Nacional Autónoma de México, Instituto de Investigación en Materiales, Circuito Exterior s/n, Ciudad Universitaria, A.P. 70-360, Del. Coyoacán, C.P. 04510 México, D.F. Mexico*
[c] *Instituto Politécnico Nacional, Grupo de Ingeniería en Procesamiento de Materiales CICATA-IPN, Unidad Altamira. Km 14.5, Carretera Tampico-Puerto Industrial Altamira, C.P. 89600. Altamira, Tamps., Mexico*

Received 18 August 2006; received in revised form 20 April 2007; accepted 12 October 2007

Abstract

The electrochemical performance of IrO_2/yttria stabilized zirconia (YSZ) cermet cathodes for solid oxide fuel cells was experimentally evaluated in relation to their microstructure. Noble metal films were prepared by MOCVD using metal–acetylacetonate precursors which were mixed and evaporated together (493 K) to achieve codeposition. The effects of experimental conditions on deposition rates, composition and microstructure were studied, and the optimum conditions were determined. The growth of the films was columnar and layered in structure, with porous morphology. TEM observations revealed that the IrO_2–YSZ composites are constituted by single-phase particles, between 4 and 10 nm in size, with an excellent composite distribution. The cathode-related polarization resistance, Rp, was measured by impedance spectroscopy and found to be in the range of 21–968 Ω cm^2 under the experimental conditions (573–873 K). IrO_2–YSZ electrodes undergo structural and/or morphological changes caused by cathodic polarization and high temperature (873 K). However, this behavior could contribute to the improvement of the electrochemical performance of the electrode. IrO_2–YSZ films displayed superior electrochemical properties as electrodes to zirconia electrolytes than that exhibited for the Pt–C and conventional Pt paste electrodes.

Keywords: IrO_2–YSZ; Nanocomposites; MOCVD; Thin films

1. Introduction

Ionic–electronic composites have wide applications in solid-state ionic devices such as batteries, gas sensors, membranes for gas separation, and fuel cell electrodes [1–4]. Ionic–electronic mixtures are also potential electrode materials for solid oxide fuel cell (SOFC) electrodes. The SOFC is an all-solid state fuel cell consisting of two porous ceramic electrodes separated by a dense oxide ion-conducting ceramic electrolyte. SOFC electrodes require, for instance, thermal stability, thermal expansion match with electrolyte, fast electrode kinetics and electrode catalytic effects [4,5]. It has been found that composite electrodes synthesized from ionically conducting particles and electronically conducting particles can increase the triple phase boundary (TPB), which reduces the electrode resistance of SOFC [6,7]. TPB is only electronically active if gas, electrons and oxide ions can percolate through pores, electrode and electrolyte. Since the microstructure affects the extension of active TPB, as a consequence, it determines the overall reaction rate [8–10]. On the other hand, electrodes should have high electronic conductivity, good chemical/thermal stability and high catalytic activity also for the dissociation of oxygen molecules [11–14]. Platinum group metals [15], Ni [16] and lanthanum strontium manganite (LSM) [17] could satisfy these requirements. LSM has been considered one of the most promising cathode materials for SOFCs due to its good performance at low temperatures; however, the related cathode

* Corresponding author.
E-mail address: atohuer@hotmail.com (A.M. Torres-Huerta).

0167-2738/$ - see front matter © 2007 Elsevier B.V. All rights reserved.
doi:10.1016/j.ssi.2007.10.010

overpotential remains significant in these kinds of fuel cells. Besides, Pt has been generally used as electrode in SOFC and oxygen sensors; however the operation temperature of a Pt/YSZ/Pt sensor is above 800 °C, due to low catalytic activity, and slow charge transfer reaction at the electrode–electrolyte–gas triple phase boundary [14]. Lately, reducing temperature and the overpotential of the cathode in solid oxide fuel cells (SOFCs) are attracting extensive interest because of their potential applications to the automobile power units and compact-size co-generation units [18]. As a candidate cathode material, lanthanum cobaltite (LSCF) has been investigated widely [18–20]. LSCF reduce the cost by lowering the operating temperature which enables the use of relatively cheap metallic interconnects and balance of the plant equipment. However, by decreasing the operating temperature, the electrode resistivity is exponentially increased and the performance of the cell is reduced. For intermediate temperature operation, reasonable performance has been reported for the electrolyte and anode, but problems remain for cathode, i.e., the mismatch of thermal expansion and the reaction with zirconia are obstacles for its use on yttria – (YSZ) or Scandia (SSZ) – stabilized zirconia electrolytes. Ir and IrO_2 are other probable candidates for cathodes because of their high catalytic activity for reduction/oxidation of oxygen [14,21]. Even though Ir is as highly priced as Pt, an Ir+oxygen combination displays a high chemical inertness, can reduce the operating temperature and overpotential of the fuel cells and gives ohmic conductivity comparable to that of common metals [21]. Therefore, in this paper, we have synthesized nanocrystalline IrO_2–YSZ composites by metalorganic chemical vapour deposition (MOCVD), in order to use them as electrodes in zirconia-based devices. Ir, YSZ, and IrO_2–ZrO_2 thin films were also prepared as a reference. The effect of the conductivity and operation temperature on the SOFC devices was analyzed. Nanocrystalline nature and morphology of the electrodes were determined by using transmission electron microscopy (TEM) and scanning electron microscopy (SEM).

2. Experimental procedure

2.1. Cermet preparation

$(CH_3COHCHCOCH_3)_3Ir$ (40 mg)+$(CH_3COHCHCOCH_3)_4Zr$ (70 mg)+$(CH_3COHCHCOCH_3)_3Y$ (10.5 mg), good purity (97–98%) were ultrasonically mixed and used as precursors to prepare IrO_2–YSZ nanocomposites. Polished quartz and glass plates 12×10 mm in size with a thickness of 2 mm were used as substrate. A schematic diagram of horizontal hot-wall MOCVD reactor is depicted in Fig. 1a. In order to determine optimal conditions for IrO_2–YSZ cermets, thin films of Ir, YSZ and IrO_2–ZrO_2 were also synthesized. The experimental conditions for IrO_2–YSZ nanocomposites evaluated in this study were: oxygen as carrier and reactive gas with a flow rate of 7.8 L h^{-1}. The deposition temperatures (T_{dep}) were analyzed between 773 K and 873 K, at 133.3 Pa. The experiments were usually performed during 25 min. The crystal structure was analyzed by X-ray diffraction (XRD, Siemens D5000) using Cu-Kα radiation without filter. Morphology and texture were examined by scanning electron microscopy using a SEM, JEOL JSM-6300 apparatus. Thickness and phase composition of the nanocomposite electrodes were examined by transmission electron microscopy (TEM, JEOL-2000 FX-II). During TEM measurements the nanocomposites were deposited in a NaCl monocrystal in order to diminish support interference.

During electrochemical measurements YSZ was used as electrolyte. YSZ pellets were produced by pressing and sintering YSZ powder (8 mol%-Y_2O_3–ZrO_2 by Hokko Corp.). Samples with 1.5 cm diameter and 0.13 cm thickness

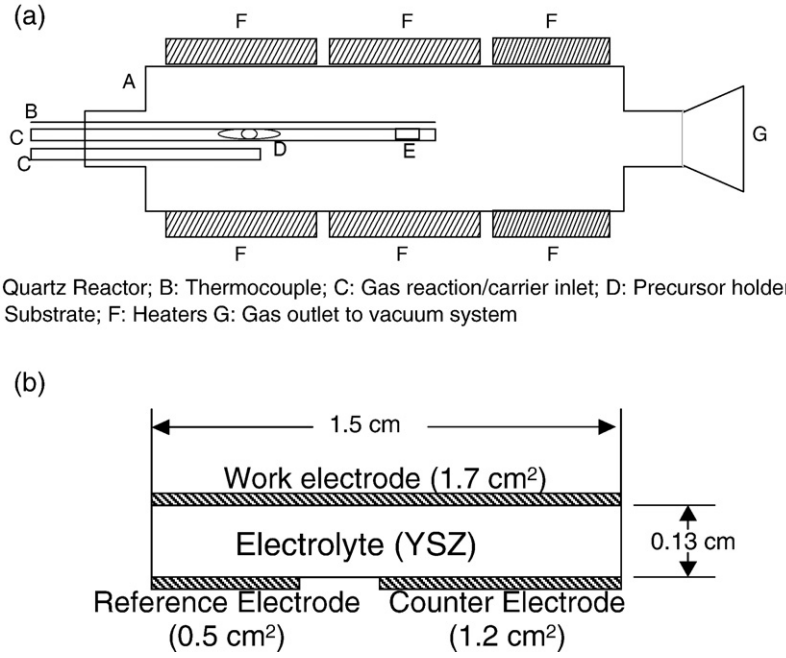

Fig. 1. a) Experimental setup and b) cell configuration.

were obtained after sintering in air at 1673 K for 5 h. Then, gold wires were bonded to both sides of the pellets. Once the electrolyte was prepared, thin films of IrO_2–YSZ were deposited at the experimental conditions previously found. The as-formed IrO_2–YSZ nanocomposite electrodes on YSZ pellets were placed in a quartz tube, which was introduced into a tube oven and tested in air, in order to determine their electrochemical properties by a three terminal method. The deposited films were considered to be completely homogeneous, therefore current densities and impedance values were calculated based on the geometric areas. The active area for the working electrode was 1.7 cm^2 (one side of the YSZ pellet) while on the opposite side the geometric areas were 0.5 cm^2 and 1.2 cm^2 for reference and counter electrodes, respectively (Fig. 1b). Tafel parameters were calculated from linear polarization curves. These curves were carried out ±400 mV from open circuit potential (E_i=0) at a scan rate of 1.67 mVs^{-1}, using a potentiostat/galvanostat model 263A (EG&G) with an impedance/gain-phase analyzer interface (Solartron SI 1260). All the experiments were conduced in the temperature range of 573–873 K and are reported versus standard hydrogen electrode (SHE).

The electrical properties were measured by AC impedance in the frequency region of 10^5 to 10^{-2} Hz in air (4 frequency points per decade). The signal applied to the cell was generally 10 mV r m s. The real (Z') and imaginary (Z'') components of impedance spectra in the complex plane were analyzed using nonlinear least squares (NLS) fitting program to estimate the parameters of grain boundary resistance (R_s), charge transfer resistance (R_{ct}) and double layer capacitance (C_{dl}).

3. Results and discussion

Optimal conditions for IrO_2–YSZ cermets and thin films of Ir, YSZ and IrO_2–ZrO_2 as a reference are shown in Table 1. As can be seen, Ir conditions were adjusted to zirconium oxide thin film conditions reach composite codeposits. The range of temperatures 473–493 K was found the upper limit of thermal stability of metal complexes with organic ligands in condensed phase. The metallic ratios were also adjusted to obtain IrO_2–YSZ cermet composites as some researchers have published [22].

3.1. Structural characterization

3.1.1. XRD

The microstructural properties of the codeposits were analyzed by X-ray diffraction (XRD). Fig. 2a and b shows final XRD patterns for Ir thin films obtained at 773 and 823 K, using amorphous glass as substrate. Silver-colored films well adhering to the substrates were obtained under the experimental conditions. The characteristic reflections were compared to JCPDS 06-0598 cards. It may be observed that the XRD peaks for synthesized samples at 823 K were broader than those obtained at 773 K. These broader peaks may imply smaller grain sizes forming the film at higher temperatures (873 K), however, some carbon deposits were also observed and, as a consequence, it appears that the grown film was not uniform at this temperature. In fact, it could be observed that XRD patterns at this temperature displayed an amorphous region (from 2θ=20 to 40), which corresponds to the substrate response. It can also be seen that, the deposits grew with some preferred orientation in the planes (111) and (200).

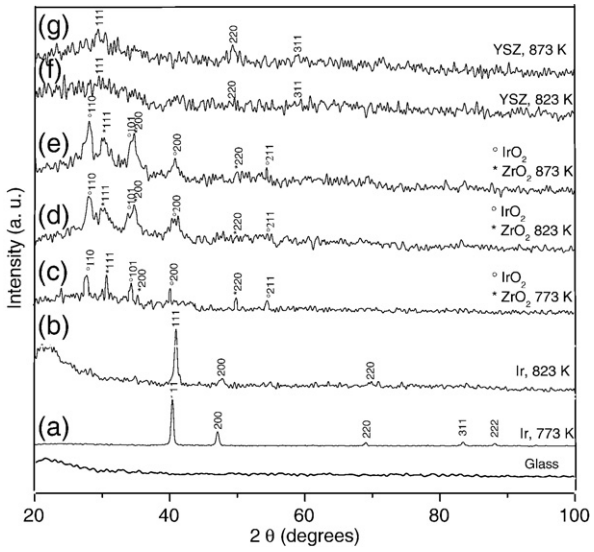

Fig. 2. XRD patterns of Ir (773–823 K), YSZ (823–873 K) and IrO_2–ZrO_2 (773–873) thin films.

As it is known, the decomposition temperature in vacuum of the Iridium(III)-acetylacetonate is around 678 K, and in this work an optimal deposition temperature was found to be 773 K. Temperatures higher than this value reduced grain size, but increased the film contamination (carbon content). This may indicate that the M–O bonds between the metal and the ligand are of comparable strength to the internal C–C bonds of the ligands. Therefore, the ligand decomposes together with the metal complex at 873 K and the formed film is highly contaminated with carbon [23–25]. This carbon contamination arising from the decomposition of the acetylacetonate ligands also caused small porous on the surface.

Fig. 2c, d, and e shows XRD patterns for IrO_2–ZrO_2 composite films at 823 and 873 K. Two structural phases, cubic and tetragonal, were identified for ZrO_2 using JCPDS 27-0997 and 17-0923 cards, respectively. JCPDS 15-0870 card was also used to identify IrO_2. Combining the experimental conditions to obtain IrO_2–ZrO_2 composite films, a uniform film deposition was observed on the substrate from 823 K on. However, at 873 K the particle size was smaller than that synthesized at low temperatures, which can be appreciated in the broadening and

Table 1
Deposition conditions for composite electrodes

Thin film	Precursor temperature (K)	Deposition temperature (K)	Gas flow (cm^3 min^{-1})	Weight of precursor (mg)
Ir	473	773	180	40
YSZ	493	873	130	10.5–70
IrO_2–ZrO_2	493	823	130	40–60
IrO_2–YSZ	493	873	130	40–10.5–70

height of the identified peaks. The oxygen excess during experimental procedure was effective to suppress carbon incorporation into IrO_2–ZrO_2 cermet films. Thus, high-purity films with no detectable signals of carbon were obtained by controlling the oxygen flow rate. We believe that as a result of the oxygen presence, lower deposition temperatures were attained, although the deposition rates were also low at temperatures higher than 823 K.

The oxygen flow rate also affected the porosity of the films, and then at higher temperatures many small pores were observed on the surface.

Finally, the XRD patterns for YSZ grown films obtained at 823 and 873 K and identified with JCPDS 30-1468 card are given in Fig. 2e and f. The narrow peaks observed for YSZ deposits can be attributed to the low crystallinity of the composite film. In general, the deposited films were transparent and non-uniform, but had good adherence. It was also observed that from a weight ratio $Zr/Y = 6.69$ of the precursors, the cubic phase structure could be achieved. The MOCVD results agreed with Wang et al. [22] who has reported transparent and cubic structure for YSZ thin films by means of aerosol assisted chemical vapor deposition. This information may indicate that under these experimental conditions, yttria stabilizes the high-temperature cubic fluorite structure of zirconia and it could increase its oxygen vacancy concentration; which enhances ionic conductivity and leads to an extended oxygen partial pressure range for ionic conductivity. Therefore, YSZ films could possess adequate oxygen ion conductivity in oxidizing and reducing atmospheres; a quality highly desired in industrial applications.

Fig. 3 shows XRD typical patterns of IrO_2–YSZ nanocomposite films, illustrating the structural characteristics evolved during the electrode fabrication. The optimal temperature for this composite was reached at 873 K. In these cermets, the IrO_2 content was fixed at 35 wt.% (based on the metallic Ir). As is shown, the grains forming the film were randomly oriented; the reflections were broad and could be correlated to either the overlapping of the IrO_2 and YSZ characteristic planes, or the particle size, or both. Although YSZ seems to be in the cubic phase, the tetragonal phase can not be discarded, because the diffraction peaks of these phases are close and they could be

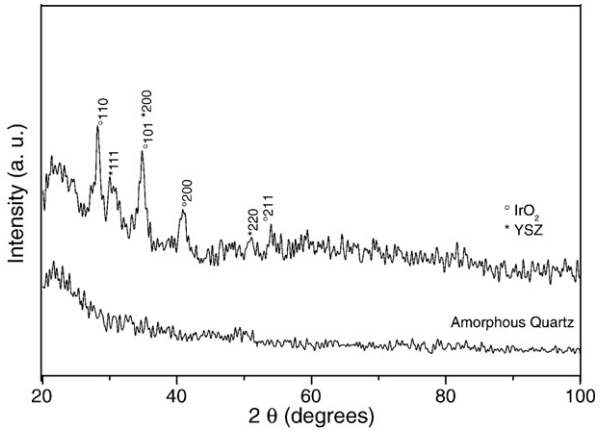

Fig. 3. Structural characterization of IrO_2–YSZ thin films.

Table 2
Average crystallite size

Electrode	Optimum deposition temperature (K)	Crystallite size (nm)
Ir	773	30
IrO_2–ZrO_2	873	25–30
IrO_2–YSZ	873	15–25

overlapped. The broad peaks as well as some narrow ones, observed for IrO_2–YSZ composites could indicate that the grown film consist of crystalline IrO_2 and quasi crystalline YSZ grains. It was found that the variation in the codeposit temperatures produces variations in the IrO_2–YSZ particles sizes and deposition rate too. It was also observed that the films were carbon free. Thus, oxygen considerably reduces the carbon contamination while, at the same time, it improves the film properties; principally, the electrical conductivity associated to the electrode/electrolyte interface.

The particle size of Ir, IrO_2–ZrO_2, IrO_2–YSZ thin films was estimated using Scherrer's equation, subsequent to the correction for instrumental broadening (see Table 2). A gradual increase in the crystallite size of Ir, IrO_2–ZrO_2, IrO_2–YSZ was observed at low temperatures. The grain sizes were approximately 30, 20, 15 nm for Ir, IrO_2–ZrO_2, IrO_2–YSZ, respectively, at higher temperatures. The morphology and catalytic activity enhanced by these nanocomposites is discussed below.

3.2. SEM and TEM observations

Fig. 4a and b shows the SEM photographs illustrating the morphological surface evolving during the film formation at 873 K. The surface texture of the films became more granular and rougher at higher temperatures. These deposits were composed of agglomerates in the sub-micron range. The dark areas in the micrographs correspond to small pores on the surface, while the gray and white areas correspond to IrO_2 and YSZ compounds, respectively (Fig. 4a).

The presence of fractured surfaces (cracks) may also be observed due to the different thermal expansion coefficient from quartz to IrO_2–YSZ cermet composites (Fig. 4b). These micrographs indicated that both IrO_2 and YSZ compounds are crushed to each other to form irregular-shaped particles, of which the average size was between 10 and 20 nm. Additionally, it seems that gray and white nanocomposites covered almost uniformly the surface substrate. One noticeable feature here is that both components forming the cermets displayed similar particle size and only can be distinguished by SEM or TEM measurements. Furthermore, the films grew with significant porosity, uniform thickness, and an even distribution of both components. In spite of these observations, it seems to be that adhesion properties of the film were not affected, and deposits showed good adherence.

Fig. 4c shows the cross sectional texture of IrO_2–YSZ cermets obtained by SEM measurements. The micrograph shows a compact columnar-type layered microstructure forming a rough but uniform surface. The grown film showed fine pores

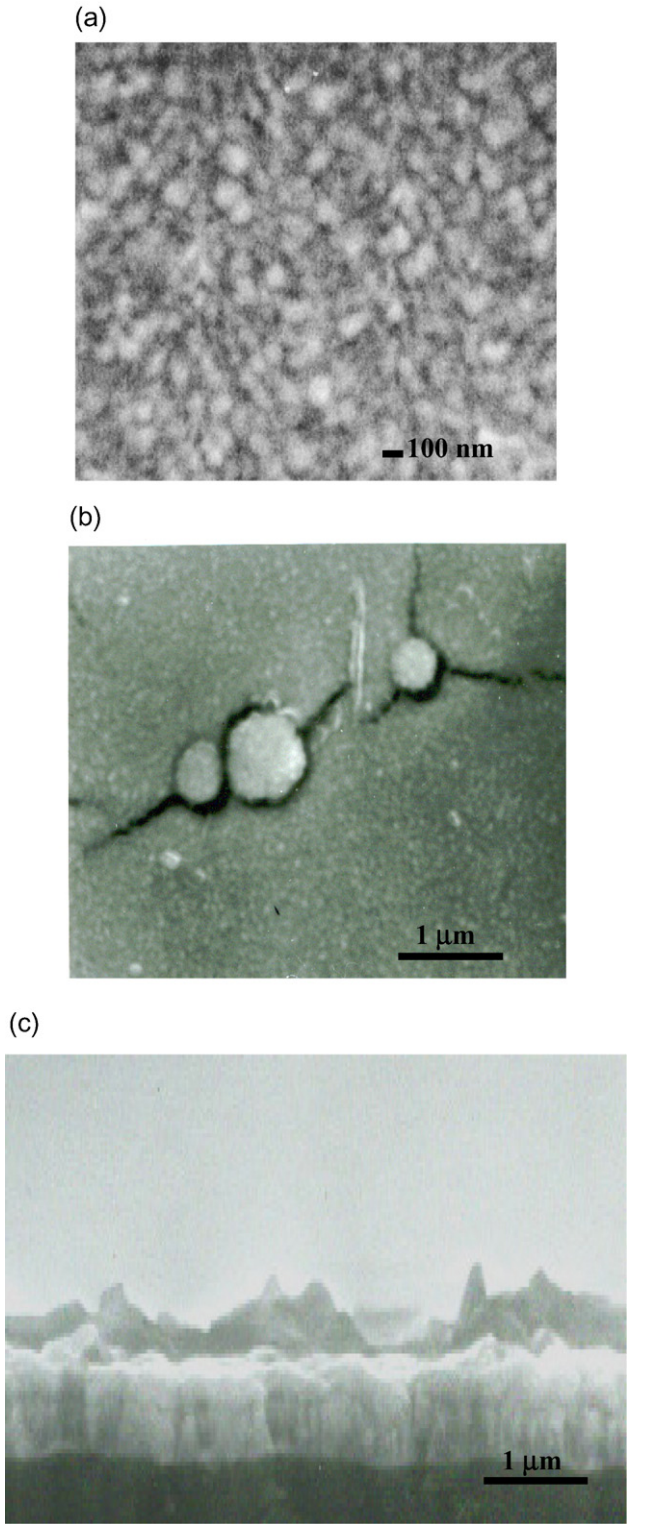

Fig. 4. SEM micrographs showing morphology and structure of IrO_2–YSZ cathodes at 20 kV and (a) 40,000× b) 13,000× and c) thin film cross section, 6500×.

with cracks. This region of the cermets was well-defined against the underlying bulk substrate. This porous film had a fairly constant thickness of the order of 1 μm. The particles and pores produced in these films were much smaller than those obtained by IrO_2 and YSZ depositions.

The nanosized nature of the thin film formation was determined by transmission electron microscopy (Fig. 5a and b). TEM observations revealed that the films consisted of two phases (grey and white), which are uniformly distributed to integrate the nanocomposites. According to EDS analysis, the dark area corresponds to IrO_2 particles that combined or dispersed on cubic YSZ. Selected area diffraction patterns confirm nanometric average particle size obtained during CVD process for IrO_2–YSZ cermet composites (figure insert). The mean particle size of the agglomerates was about 4–10 nm in diameter. These observations are in good agreement with SEM analysis. The nano-scale of every single component observed in Fig. 5a and b was consistent with the broadening of the XRD reflections. The electron diffraction pattern of the cermets is characteristic for a nanocrystalline material. Broader and diffuse electron diffraction rings (not shown here) were obtained at low temperatures, which can be attributed to the low crystallinity of YSZ particles and an increase in particle size.

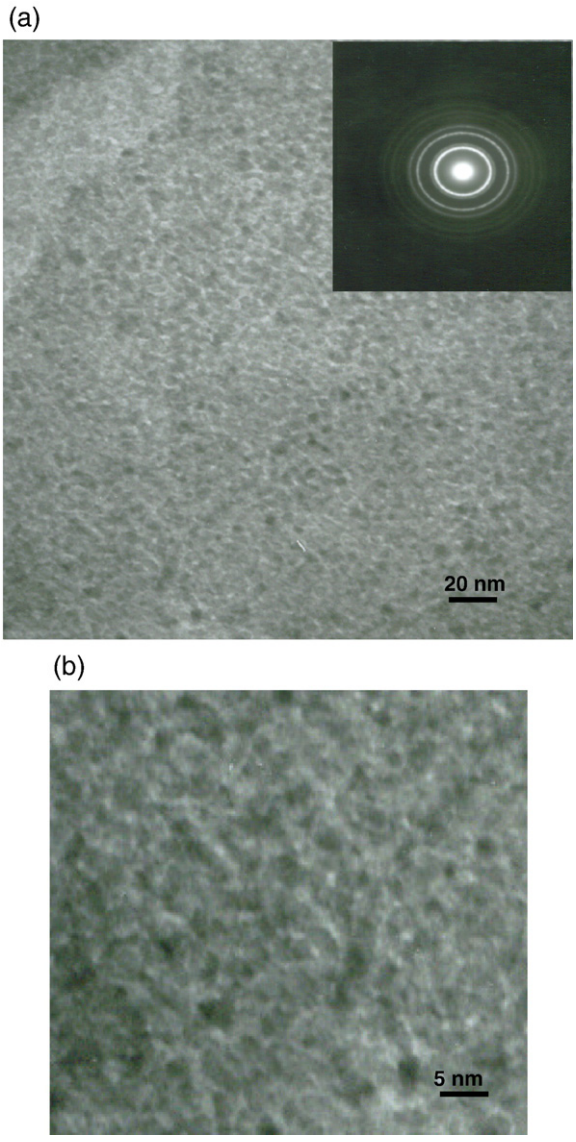

Fig. 5. TEM images of IrO_2–YSZ composite thin films at 200 Kv. a) 250 Kx and b) 400 Kx.

3.3. Electrochemical measurements

3.3.1. Polarization curves

Fig. 6 shows polarization curves for IrO_2–YSZ composites in air at different temperatures. The electrochemical behavior of cathodic and anodic polarization curves was quite similar; however, a positive displacement of the equilibrium potential, E_{eq}, towards more active values at higher temperatures can be observed. This behavior can be explained by the fact that the activity of IrO_2–YSZ cermets was controlled by charge transfer reactions and, as a consequence, there is only one Tafel slope associated with the oxygen reduction occurring at the triple phase boundary. In this study, the geometric area has been considered a good approximation, while the largest possible surface area was not determined, which affect directly current density values, therefore, this could explain the higher Tafel slopes that were found during the experiments (Table 3). The influence of the temperature on the exchange current densities (I_o) are also presented in this table. The Tafel slopes and I_o values seem to be reproducible within a factor of 1.5 and the reported values are an average of three measurements. From these results, it was clear that the overall current passing through the system increased with the temperature. Polarization results indicated that a sufficiently large fraction of the electrolyte surface was accessible for charge transfer. If it is assumed that three-phase boundaries (TBP) will be in mutual contact and would be places where the charge transfer occurs more easily, then the fraction of the electrolyte area that will be accessible for charger transfer in industrial applications is determined by the electrode microstructure. Thus, the inhomogeneity es observed during Tafel curves could be attributed to the porosity and cracks that could extend up to electrolyte during thin film formation, as has been determined by SEM and TEM measurements. Comparing exchange current densities reported for Pt at similar temperature [26], in IrO_2–YSZ cermets a comparable electrochemical performance as Pt electrodes can be appreciated, however, our samples were almost carbon free, while Pt films containing approximately as much carbon as Pt.

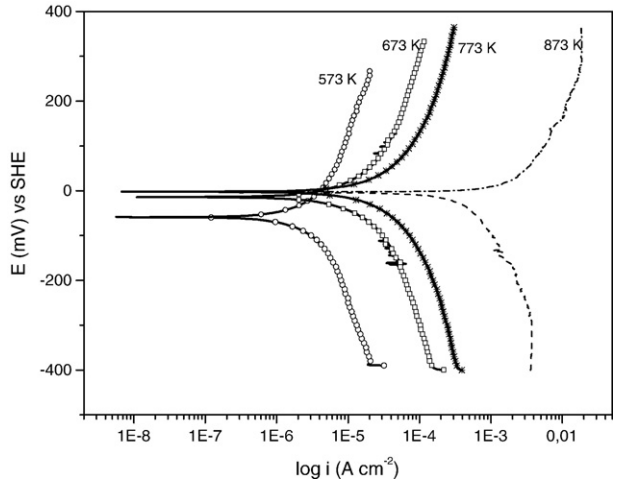

Fig. 6. Tafel curves for the IrO_2–YSZ cermets.

Table 3
Exchange current densities (I_o) and Tafel slopes for IrO_2–YSZ electrodes

Temperature (K)	IrO_2–YSZ	
	Log I_o (A cm^{-2})	m (mV decade^{-1})
573	−5.56	−213
673	−4.70	−206
773	−4.27	−206
873	−3.28	−253

3.3.2. EIS measurements

Typical ac impedance spectra observed with IrO_2–YSZ composites at different temperatures are shown in Fig. 7, where the equivalent circuit is shown in the figure insert. In the electrochemical impedance results, the data corresponding to the bulk and grain boundary of the electrolyte are out of the frequency scale (10^5–10^{-2} Hz) [27].

The spectra at 573 and 673 K exhibited a tendency to form a typical semicircle, while at 773 and 873 K, a well formed semicircle can be observed, which can be attributed to the thin film impedance. A tenuous deformation (tail) can also be observed at low frequencies. This small tail can be explained by a small increment in the particle size, which can cause a modification of electrode microstructure at operation temperature [27]. This dispersion can also be attributed to some interfacial reactions that occur during the process. The results demonstrated an enhanced in the electrocatalytic activity, and this behavior is comparable to values published elsewhere [26,28]. In fact, temperatures higher than 773 K displayed slightly better activity than those reported for other composites [6,14].

It is well known, that in a wide range of electronically and ionically conducting materials, both crystalline and amorphous, an ideal Debye-like response is never obtained [27]. Therefore, there are various approaches for modeling the non-ideality and, in particular, the functional form of the high frequency response. In this case, we used a combination of equivalent circuits, with the implicit inclusion of all electrically active components together with constant phase elements, to represent the departures from Debye-like ideality of each component.

The inserted figure highlights the equivalent circuit models used for the study of the IrO_2–YSZ nanocomposites. In general, the data points showed similar features at the analyzed frequencies with typical depressed semicircles which have been described by the following equation [27,28]

$$Z(j\omega) = R_s + \frac{R_{ct}}{[1\{-j\omega C_f R_{ct}]^{\alpha}} \quad (1)$$

where Z is the complex impedance, R_s is the grain boundary resistance, C_f is the film capacitance, ω is the angular frequency, R_{ct} is the film porous resistance, $j=(-1)1/2$, and $0<\alpha\leq 1$. α is an empirical term to account for the depression of the semicircle.

The spectra were deconvoluted with the equivalent circuit, and fitting values are shown in Table 4. As may be observed, the capacitance, as well as charge transfer resistance values, decreased at high temperatures, which is desirable in a commercial application. The capacitance values can be associated to the

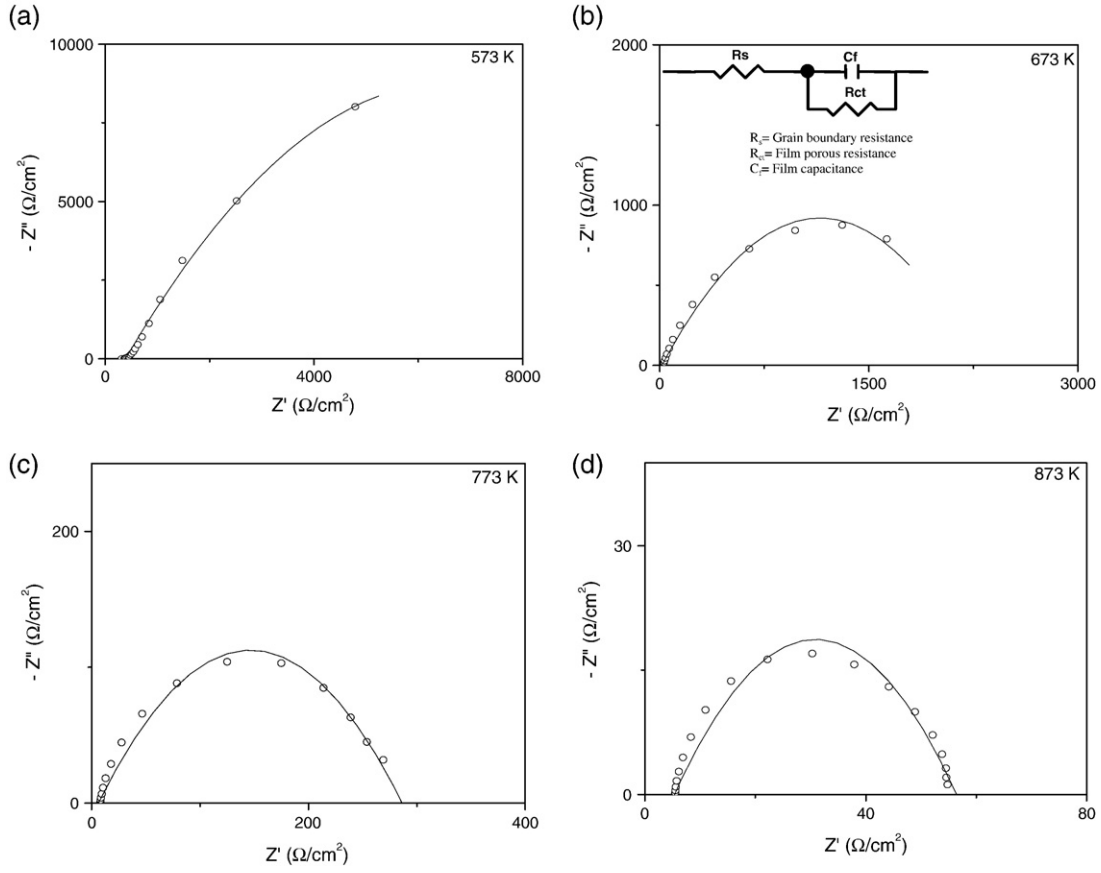

Fig. 7. ac impedance spectra of IrO_2–YSZ composites at a) 573, b) 673, c) 773 and d) 873 K.

oxygen ion transfer from boundary triple points to the electrolyte, which agree with previous researches [27]. The observed spectra behave similar to each other depending on the operation conditions, reflecting that the electrochemical properties of cermet electrodes critically depend on their microstructures (number of reaction sites, porosity, electrode/electrolyte adhesion, etc.) or temperature operation or both. Furthermore, it can be seen that the grain boundary resistance becomes negligible at higher temperatures, indicating that the diffusion was only through a layer of finite thickness.

A high dependence of Rp values on temperature was observed from 21 to 968 Ω cm^2. Apparently, there were some structural and morphological changes of IrO_2–YSZ cermets when the temperature was increased. The significant differences in Rp values measured in the present work indicate that ionic resistance in the electrolyte phase of the cermet contributes significantly to Rp at low temperatures.

Table 4
Fitted results of EIS spectra for IrO_2–YSZ thin films evaluated at different temperatures

Temperature (K)	R_s (Ω cm2)	R_{ct} (Ω cm2)	Capacitance (μF)
573	560.0	15,900	5151
673	42.7	3250	1055
773	6.5	311	142
873	5.3	50	100

The Arrhenius plot for the conductivity associated with the total electrode resistance for IrO_2–YSZ composites along with that exhibited by other types of composite electrodes obtained by MOCVD are shown in Fig. 8 [29]. The total electrode resistance was represented by the contribution of electrochem-

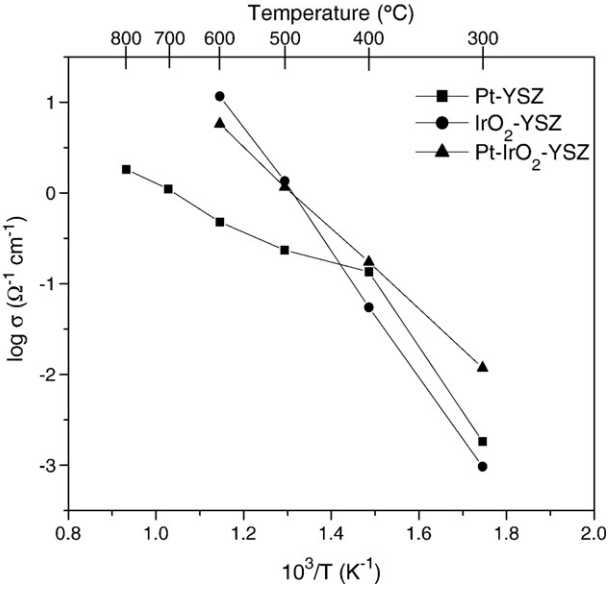

Fig. 8. Arrhenius plot for the conductivities associated to the total electrode resistance.

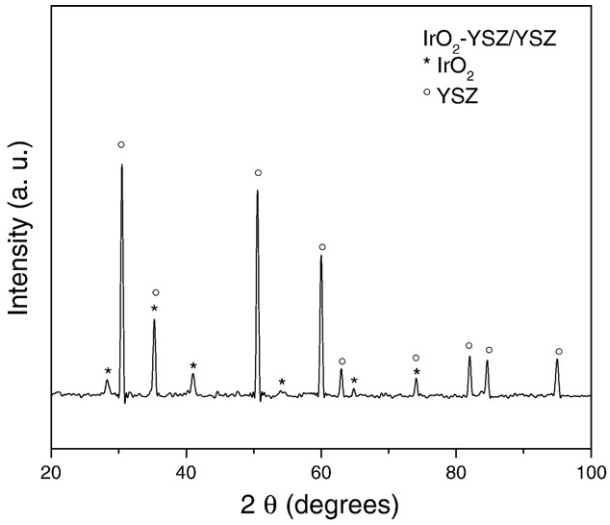

Fig. 9. XRD patterns of IrO_2–YSZ thin film over YSZ pellet after the electrochemical tests.

ical reaction components. IrO_2–YSZ electrode films displayed the highest conductivity; higher even than those for Pt [30,14] and Ir–YSZ [14] conventional electrodes. At the experimental conditions, the activation energy for the interfacial conductivity of the IrO_2–YSZ composites was about 85 kJ mol^{-1}, which is in good agreement with the activation energy of the dissociation of oxygen molecules.

The results indicate that the nanocrystalline nature of IrO_2–YSZ thin films may considerably increase the number of the triple phase boundaries electrolyte–electrode–O_2 in air, where the charge–transfer reactions takes place; reducing temperature operation in electrochemical devices.

Barbucci et al. [31] have analyzed the differences between chemical–physical properties of Pt and LSM cathodes. They found that the kinetic of oxygen reduction is faster on LSM cathodes than for Pt cathodes, and that the activation energy for LSM cathodes was about 100 kJ-mol^{-1}. In addition, the authors did not observe significant changes when the content of the ionic conductor was modulated or modified with YSZ. On the other hand, the activation energy of the Pt electrode changed from values of 150 kJ-mol^{-1} to about 90 kJ-mol^{-1} when YSZ was introduced into the electrode. Considering that the values of 100 and 150 kJ-mol^{-1} are fairly consistent with the literature results for LSM and platinum electrodes, the IrO_2–YSZ cermets synthesized in this work may offer an efficient and competitive performance as electrode materials when YSZ is used as electrolyte.

In order to determine changes in the microstructure of the electrode after electrochemical measurements XRD studies were carried out (Fig. 9). The response corresponding to YSZ in the composite overlapped with the YSZ electrolyte changes in the width and intensity of the peaks were observed for IrO_2. The XRD response could be attributed to an increasing of the IrO_2 particle size, or to the dissolution of IrO_2 in the electrolyte layer, as Kim et al. [32] suggested.

The results discussed above suggest that IrO_2–YSZ electrodes suffer structural and/or morphological changes caused by the cathodic polarization and the temperature (873 K). However, this behavior could contribute to the improvement of the electrochemical performance of the IrO_2–YSZ electrodes, as has been reported by Jiang and Love [33], who found that structural changes in SOFC electrodes could promote the O_2 reduction reaction. However, further studies will be required in order to determine how these changes affect the performance of these electrodes. In addition, long-term tests designed to determine the stability of the electrode and its performance in industrial applications will be discussed in future works.

4. Conclusions

IrO_2–YSZ composite films consisted of IrO_2 and YSZ particles between 4 and 10 nm were obtained by MOCVD. The growth of the films was columnar and layered in structure, with porous morphology. The electrical conductivity assigned to the response of the composites was higher than that for conventional Pt paste electrodes due to an increase in the triple phase boundaries (electrolyte–electrode–O_2). Properties of the thin films (i.e., high three-phase boundaries adherence and stable microstructure) can be predicted from the impedance measurements. From the electrochemical and structural results, it can be concluded that, given the good response displayed for the material, further microstructural analysis during operation process is required in order to determine if the IrO_2–YSZ composite films could be used as electrodes in YSZ electrolyte.

Acknowledgments

The authors are thankful for the financial support from CGPI-IPN and SNI-CONACYT.

References

[1] C.C. Lian, A.V. Joshi, N.E. Hamilton, J. Appl. Electrochem. 8 (1978) 445.
[2] A. Menne, W. Weppner, Electrochim. Acta 11-12 (1991) 1823.
[3] Z. Wu, M. Liu, Solid State Ionics 93 (1997) 65.
[4] N.Q. Minh, J. Am. Ceram. Soc. 76 (1993) 563.
[5] E. Ivers-Tiffée, W. Wersing, M. Schiessl, Ber. Bunsenges. Phys. Chem. 94 (1990) 978.
[6] Y. Min Park, G. Man Choi, Solid State Ionics 120 (1999) 265.
[7] T. Kenjo, M. Nishiya, Solid State Ionics 57 (1992) 295.
[8] M.J.L. Ostergard, C. Clausen, C. Bagger, M. Mogensen, Electrochim. Acta 40 (1995) 1971.
[9] K. Sasaki, J. Gauckler, in Proc. Int. Symp. Struct. Func. Grad. Mater. 3 (1995) 651.
[10] M. Juhl, S. Primdahl, C. Manon, M. Mogensen, J. Power Sources 61 (1996) 173.
[11] F.C.T. So, E. Kolowa, X.-A. Zhao, E.T.-S. Pan, M.A. Nicolet, J. Vac. Sci. Technol. B5 (1987) 1784.
[12] E. Kolowa, F.C.T. So, E.T.-S. Pan, M.-A. Nicolet, Appl. Phys. Lett. 50 (1987) 54.
[13] A. Belkind, Z. Orban, J.L. Vossen, J.A. Woollam, Thin Solid Films 50 (1992) 242.
[14] T. Kimura, T. Goto, Surf. Coat. Technol. 198 (2005) 36.
[15] K. Sasaki, J. Tamura, M. Dokiya, Solid State Ionics 144 (2001) 223.
[16] M. Mogensen, S. Skaarup, Solid State Ionics 86-88 (1996) 1151.
[17] M.J. Jorgensen, S. Primdahl, M. Mogensen, Electrochim. Acta 44 (1999) 4195.

[18] S.C. Singhal, in: O. Yamamoto, Y. Takeda, S. Noda, S. Kawatsu, N. Imanishi (Eds.), Int. Symposium on Fuel Cells for Vehicles, Electrochem. Soc. Jpn., Tokyo, , 2000, p. 109.
[19] J.M. Bae, B.C.H. Steele, Solid State Ionics 106 (1998) 247.
[20] E. Maguire, B. Gharbage, F.M.B. Marques, J.A. Labrincha, Solid State Ionics 127 (2000) 329.
[21] S. Music, S. Popovic, M. Malijkovic, Z. Skoko, K. Furic, A. Gajovic, Mater. Lett. 57 (2003) 4509.
[22] H.B. Wang, C.R. Xia, G.Y. Meng, D.K. Peng, Mater. Lett. 44 (2000) 23.
[23] J.R. Vargas-Garcia, T. Goto, Mater. Trans. 44 (9) (2003) 1717.
[24] I.K. Igumenov, J. Phys. IV Colloq. C5 (5) (1995) C5–489.
[25] A. Zinn, B. Niemer, H.D. Kaesz, Adv. Mater. 4 (5) (1992) 375.
[26] J.A. Montes de Oca, J.R. Vargas, J. Godinez, E.M. Arce, V. International Congress of Materials and XX. Metallurgical Research Meeting, México, 1998, p. 380.
[27] J.T.S. Irvine, D.C. Sinclair, A.R. West, Adv. Mater. 2 (3) (1990) 132.
[28] R. Cottis, S. Turgoose, Electrochemical impedance and noise, NACE International, 1999.
[29] A.M. Torres-Huerta, J.R. Vargas-Garcia, J. Metastable Nanocryst. Mater. 24-25 (2005) 399.
[30] S.P.S. Badwalle, H.J. de Bruin, Phys. Status Solidi A, Appl. Res. 54 (1979) 261.
[31] A. Barbucci, R. Bozzo, G. Cerisola, P. Costamagna, Electrochim. Acta 47 (2002) 2183.
[32] S-H. Kim, D-Y. Park, H-J. Woo, D-S. Lee, J. Ha, C-S. Hwang, J. Mater. Res. 17 (2002) 1735.
[33] S.P. Jiang, J.G. Love, Solid State Ionics 158 (2003) 45.